

Crystal-to-Crystal Synthesis of Photocatalytic Metal–Organic Frameworks for Visible-Light Reductive Coupling and Mechanistic Investigations

Luis Gutiérrez,^[a] Suwendu Sekhar Mondal,^[a] Alberto Bucci,^[a] Noufal Kandoth,^[a] Eduardo C. Escudero-Adán,^[a] Alexandr Shafir,^[b] and Julio Lloret-Fillol^{*[a, c]}

Postmodification of reticular materials with well-defined catalysts is an appealing approach to produce new catalytic functional materials with improved stability and recyclability, but also to study catalysis in confined spaces. A promising strategy to this end is the postfunctionalization of crystalline and robust metal–organic frameworks (MOFs) to exploit the potential of crystal-to-crystal transformations for further characterization of the catalysts. In this regard, two new photocatalytic materials, MOF-520-PC1 and MOF-520-PC2, are straightforwardly obtained by the postfunctionalization of MOF-520 with perylene-3-carboxylic acid (PC1) and perylene-3-butyric acid (PC2). The single crystal-to-crystal transformation yielded the X-ray

diffraction structure of catalytic MOF-520-PC2. The well-defined disposition of the perylenes inside the MOF served as suitable model systems to gain insights into the photophysical properties and mechanism by combining steady-state, time-resolved, and transient absorption spectroscopy. The resulting materials are active organophotoredox catalysts in the reductive dimerization of aromatic aldehydes, benzophenones, and imines under mild reaction conditions. Moreover, MOF-520-PC2 can be applied for synthesizing gram-scale quantities of products in continuous-flow conditions under steady-state light irradiation. This work provides an alternative approach for the construction of well-defined, metal-free, MOF-based catalysts.

Introduction

Photoredox catalysis has emerged as a powerful synthetic alternative to classical thermal organic transformations.^[1] An important family of photoredox catalysts (PCs) are based on iridium, ruthenium, and copper transition metals due to their robustness and long-lived metal-to-ligand charge-transfer (MLCT) excited states.^[1e,2]

As a cost-effective alternative, organic dye PCs, such as benzophenones, cyanoarenes, quinoline, and pyrylium salts, have emerged as promising PCs based on earth-abundant elements.^[3] Additionally, simple perylene can also efficiently promote redox transformations under light irradiation.^[4]

A promising approach to further develop catalysts is to combine outstanding intrinsic activities of homogeneous systems with the chemical stability of heterogeneous ones by immobili-

zation of the catalytic sites. In some cases, catalyst immobilization leads to a reduction of performance due to the inaccessibility of active sites and mass-transport issues. On the other hand, the recyclability and stability of heterogenized catalysts generally increase. Successful examples include the coordination of PCs on porous zeolites,^[5] polymers,^[6] and metal–organic frameworks (MOFs).^[7,8] Among them, MOFs are versatile materials because they are built from organic bridging ligands and inorganic connecting points (referred to as secondary building units (SBUs)).^[10] Not only the large number of accessible SBUs,^[9] metalloligands,^[10] and organic linkers,^[11,12] but also postmodification by the encapsulation of guest molecules offer a further possibility of functionalization, such as the incorporation of photoactive molecules.^[13] As a result, the properties of the final material can be modulated to broaden the range of possible applications, from gas adsorption^[14] to sensing,^[15] light-emitting devices,^[16] biochemical systems,^[17] and heterogeneous catalysis.^[18] Therefore, MOFs are unique to design earth-abundant, metal-based, single-site solid catalyst.^[18] Still, only a limited number of MOFs have been reported to catalyze light-driven organic transformation,^[19] despite the wide variety of homogeneous PC counterparts.^[19] Those examples rely on demanding synthetic procedures, such as the synthesis of Ru^{II}- and Ir^{III}-polypyridyl complexes into UiO-type frameworks or metalloporphyrin MOFs,^[10] or the use of photoredox organocatalysts for the direct synthesis of polymers^[11,12]

A pioneering study by Yaghi and co-workers demonstrated that the coordinative alignment (CAL) of a guest molecule to the SBU of MOF-520 is an excellent methodology to allow the

[a] L. Gutiérrez,[†] Dr. S. S. Mondal,[†] Dr. A. Bucci, Dr. N. Kandoth, Dr. E. C. Escudero-Adán, Prof. J. Lloret-Fillol
Institute of Chemical Research of Catalonia (ICIQ)
The Barcelona Institute of Science and Technology
Avinguda Països Catalans 16, 43007 Tarragona (Spain)
E-mail: jlloret@iciq.es

[b] Dr. A. Shafir
Institute of Advanced Chemistry of Catalonia (IQAC-CSIC)
c/Jordi Girona 18–26, 08034 Barcelona (Spain)

[c] Prof. J. Lloret-Fillol
Catalan Institution for Research and Advanced Studies (ICREA)
Passeig Lluís Companys, 23, 08010, Barcelona (Spain)

[[†]] These authors contributed equally to this work.

Supporting Information and the ORCID identification number(s) for the author(s) of this article can be found under:
<https://doi.org/10.1002/cssc.202000465>.

postsynthetic modification and determination of a single-crystal X-ray structure and absolute configuration of bound molecules.^[20] This crystal-to-crystal modification involves the replacement of the bridging formate ligands of the SBUs with guest molecules possessing carboxylate, phenol, diol, azolate, sulfur-containing oxoacid, and phosphorus-containing oxoacid moieties.^[20]

Inspired by these studies, we hypothesized the advantage of including functional guest molecules into MOF-520, such as PCs. Coordination of the guest molecule into the SBU places the PC in a confined environment, which may allow for crystallographic characterization, and therefore, aid in providing a mechanistic understanding. Another interesting aspect of the coordination of guest molecules into MOF-520 is that the material can be considered as being composed of a collection of isolated units, and therefore, acting as single-site catalysts in a heterogeneous material. In general, mechanistic studies on heterogeneous phases are more challenging than those on homogeneous ones. However, heterogeneous reticular materials, with well-defined single catalytic sites, may serve to clarify mechanistic aspects that are otherwise tough to address in a homogeneous phase. For instance, it could be useful to elucidate the active catalytic species in PCs based on π -conjugated molecules. The tendency to form π -stacking aggregates in solution introduces an uncertainty into the catalytic species since the dynamics of excited states are very complex.^[21] In those systems, the catalytic activity can result from the monomer, the dimer, larger aggregates, or from a combination thereof.

As a proof of concept, we have anchored two different PCs in MOF-520. Perylene-3-carboxylic acid (PC1) and perylene-3-butylric acid (PC2) reacted with MOF-520 and were incorporated into the structure through a crystal-to-crystal transformation. The resulting MOFs (MOF-520-PC1 and MOF-520-PC2, respectively) showed photoredox catalytic activity for the C–C bond reductive dimerization of aromatic aldehydes, ketones, and imines, under mild reaction conditions. The diols and diamines obtained are structural motifs in natural products,^[22] pharmacologically active compounds, and auxiliaries in asymmetric syntheses.^[23] The reaction was also performed under continuous-flow irradiation and aerobic conditions to generate the bulk amount of desired products. Furthermore, the obtained MOF-520 based photocatalysts are suitable model systems to perform photophysical studies. Perylenes within the MOFs behave as single units, in contrast to the expected behavior in the homogeneous phase. We also present insights into the photocatalytic cycle obtained with the help of steady-state, time-resolved, and transient absorption spectroscopic studies.

Results and Discussion

Synthesis and structure determination

Single crystals of MOF-520 were obtained in good yield following a procedure previously reported.^[20a] As previously reported, X-ray analysis showed SBUs ($[\text{Al}_8(\mu\text{-OH})_8(\text{HCOO})_4(\text{BTB})_4]$; BTB = 4,4',4'',-benzene-1,3,5-triyl-tris(benzoate)) constituted by a ring

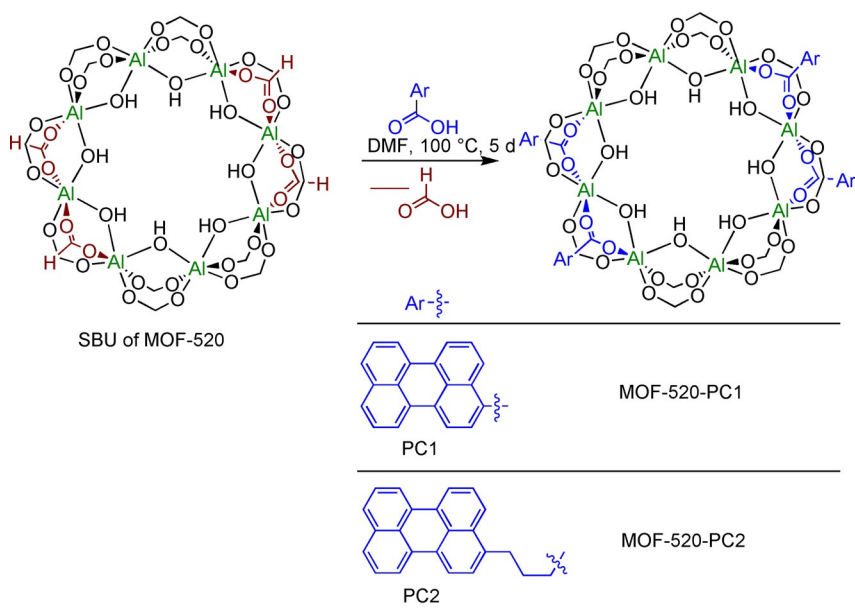
of 8 aluminum octahedra shared corners through 8 μ -OHs, 12 BTB, and 4 formate ligands, with wide window openings (13.7 Å) and cavities. Each BTB is connected to three SBUs to form a 3D porous framework. The formates are exchangeable and offer anchoring points for molecules derived from carboxylate acids.

The SBU was straightforwardly modified by incubating the crystalline white MOF-520 in DMF at 100 °C for 5 days in the presence of an excess amount of PC1 or PC2 (Scheme 1, and see the Supporting Information for details). At the end of the reaction, dark-reddish crystals were thoroughly washed with DMF and acetone and collected by filtration (Figure S1 in the Supporting Information).

The powder X-ray diffraction (PXRD) patterns of colored MOF-520-PC1 and MOF-520-PC2 exhibited sharp diffraction peaks that were identical to those of the as-synthesized sample, which indicated that the porous framework maintained its crystalline integrity (Figure 1a). Dinitrogen adsorption/desorption isotherms (77 K) of MOF-520, MOF-520-PC1, and MOF-520-PC2 indicate a decrease in porosity (Figure 1b), with BET surface areas determined to be 2438, 1448, and 1081 m²g⁻¹, respectively. The decrease of BET surface area is consistent with the steric bulk of guest perylene ligands residing in the pores of MOF-520. These MOFs exhibited reversible type I sorption curves, which were characteristic of microporous materials.

Solution ¹H NMR spectroscopy of digested MOF-520-PC1 and MOF-520-PC2 samples was performed to quantify the amount of guest catalyst binding in the bulk samples. The samples (1 mg) were transferred to a GC vial. Deuterated dimethyl sulfoxide ($[\text{D}_6]\text{DMSO}$; 0.4 mL) was added to the vial followed by the addition of NaOH (0.1 mL, 1 M in D_2O). The solution was sonicated for 5 min to digest the crystals. The vial was capped and placed in a preheated 120 °C oven for the required time to dissolve the crystals completely. The final clear solution was used to record the ¹H NMR spectrum. Perylene incorporation was determined by the ratio between the perylene and BTB linker measured in the digestion mixture (Figures S2–S4 in the Supporting Information). Based on the above results, we observed 44 and 71% of incorporation of PC1 and PC2, respectively, and could postulate the formulas $[\text{Al}_8(\mu\text{-OH})_8(\text{HCOO})_2(\text{PC1})_2(\text{BTB})_4]$ and $[\text{Al}_8(\mu\text{-OH})_8(\text{HCOO})(\text{PC2})_3(\text{BTB})_4]$, respectively.

Single-crystal diffraction of MOF-520-PC1 (Figure 2) confirmed the presence of the PC1 ligand coordinated through the carboxylate bridging two aluminum atoms (Figure S5a in the Supporting Information). The X-ray occupancy factor of the PC1 ligand was 40% (Figure 3), which was in agreement with nearly 50% formate replacement determined by ¹H NMR spectroscopy. We speculate that the full replacement of formates by PC1 is not possible due to the rigidity and steric hindrance of PC1, as determined by potential collision between neighboring PC1 positions within the same SBU (Figure S5b in the Supporting Information). MOF-520-PC1 exhibits two types of ellipsoidal pores, which are formed from elongated arrangements of SBUs (Figure S5a in the Supporting Information). The first type is an octahedral pore of $10.01 \times 10.01 \times 23.23 \text{ \AA}^3$, whereas



Scheme 1. The crystal-to-crystal reaction that proceeds by ligand exchange. Formate ligands are replaced by carboxylate-derived perylenes (PC1 and PC2) in the SBUs of MOF-520. Incoming perylene and outgoing formic acid are highlighted in red and blue, respectively.

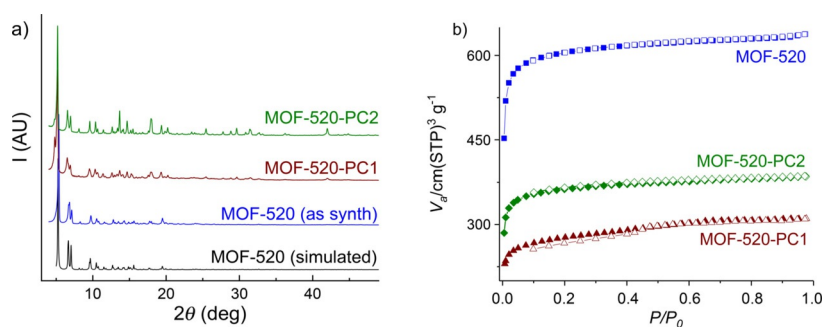


Figure 1. a) PXRD patterns and b) N_2 sorption isotherms at 77 K of MOF-520 (blue), MOF-520-PC1 (red), and MOF-520-PC2 (green). Adsorption and desorption branches are indicated by closed and open symbols, respectively.

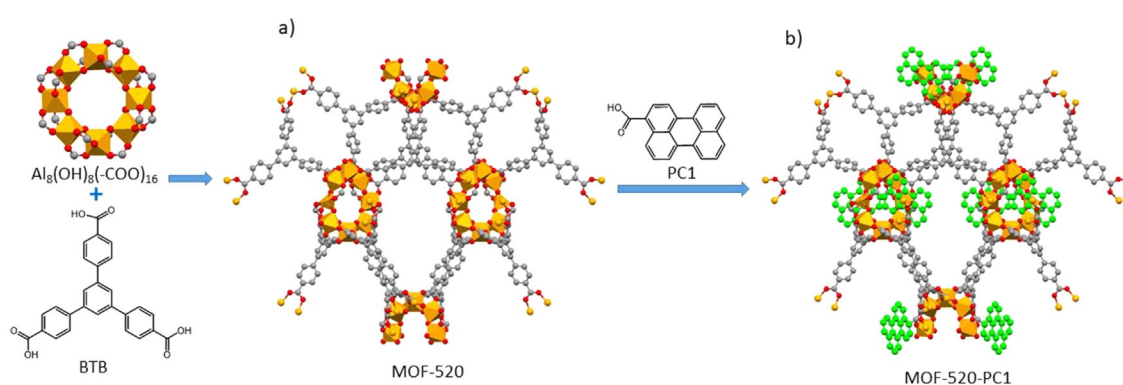


Figure 2. a) Synthesis of MOF-520 from Al-based SBUs and organic BTB linkers; the Al-based SBU is an orange polyhedron. b) The reaction of PC1 with MOF-520 leads to MOF-520-PC1. Atom color scheme: C: gray, O: red, Al: orange, perylene: green; H atoms are omitted for clarity.

the second type can accommodate an elongated tetrahedron of $5.89 \times 5.89 \times 6.21 \text{ \AA}^3$ (given the van der Waals radii of the nearest atoms).^[20a] A PLATON calculation indicates that the sol-

vent-accessible void space of MOF-520-PC1 is approximately 6000 \AA^3 , which accounts for about 50% of the crystal volume (see Figure S5 b and the animation in the Supporting Informa-

tion, which highlights the MOF cavity, windows, and encapsulated PC1). In the case of MOF-520-PC2, although single-crystal data collection was successful for the detection of PC2, it was not possible to resolve the structure, most probably due to the high degree of freedom of the flexible $-(CH_2)_3-$ units.

The strong coordination bond between Al^{3+} and the carboxylate groups, along with the high connectivity between $[Al_3]$ clusters, infers expected stability of MOF-520-PC1 and MOF-520-PC2 under different conditions. In this regard, we tested the stability of dispersed MOF samples in acetone, tetrahydrofuran, methanol, acetonitrile, dichloromethane, and DMF for 3 days at room temperature. After such treatment, the material maintained the full crystalline integrity, as confirmed by PXRD (Figures S6 and S7 in the Supporting Information).

Catalysis

To prove the photocatalytic ability of encapsulated PC inside the MOFs, we selected the light-driven pinacol coupling of a model substrate, 4-methylbenzaldehyde (**1a**). We found that suspensions of MOF-520-PC1 or MOF-520-PC2 (0.5 mol%) in CH_3CN and after irradiation with visible light ($\lambda = (447 \pm 20)$ nm) for 16 h in the presence of *N,N*-diisopropylethylamine (DIPEA) under N_2 atmosphere, yielded the corresponding pinacol **2b** in low yields (9 and 32%, respectively). These results encouraged us to optimize the conditions of the reaction (Tables S2–S4 in the Supporting Information).^[3a] After optimizing the solvent mixture (MeOH/ CH_3CN , 3:2 v/v), the yield increased up to 74 and 82% for MOF-520-PC1 and MOF-520-PC2, respectively, with 1 mol% of MOF-520-PC. Loadings of 1 mol% of MOF-520-PC are substantially lower than those previously used for homogeneous perylene organocatalysis (ca. 8–10%).^[3a] Blank experiments in the dark, without DIPEA, or without PC

(MOF-520-PC2) did not produce **2b** (Table S3 in the Supporting Information), and MOF-520 (without PC) was inactive. Interestingly, the catalytic reaction mediated by MOF-520-PC2 was also effective under aerobic conditions, giving a similar catalytic performance to that under anaerobic conditions (Table S3 in the Supporting Information). Reductive transformations under aerobic conditions are uncommon,^[24] and usually sophisticated strategies are required to avoid the reaction of O_2 with the reduced catalyst.^[25]

Subsequently, we directly compared the MOF-520-PCs with the corresponding homogeneous PCs under the best reaction conditions (Table 1). Interestingly, the heterogeneous materials exhibited similar activity to that of the homogeneous counterparts. These results suggested that most of the catalytic centers within the MOF-520-PCs were accessible and active or were enhanced in the MOF structure. Additionally, leaching experiments suggested that MOFs were robust and the primary source of the catalytic activity. The amounts of PC1 and PC2 leached were measured by UV/Vis absorption spectroscopy at the end of the catalytic run and were only about 2.3 and 1.4% for PC1 and PC2, respectively (Figures S9 and S10 in the Supporting Information).

Subsequently, we extended the scope to a broad range of aromatic aldehydes with electron-donating, electron-withdrawing, and bulky substituents. MOF-520-PC2 was the chosen catalyst for the isolation of products because of better yields. To facilitate isolation of the products, the formed diols **2a–m** were converted into the corresponding diacetates **3a–m** under standard conditions (see the Supporting Information). The formation of products was achieved in moderate to excellent yields (around 70%) under the optimized conditions (Scheme 2). Interestingly, heteroaromatic aldehydes **1l** and **1m** were found to be compatible with the reaction conditions, although they only resulted in moderate to low yields. The developed methodology was not compatible with aliphatic alde-

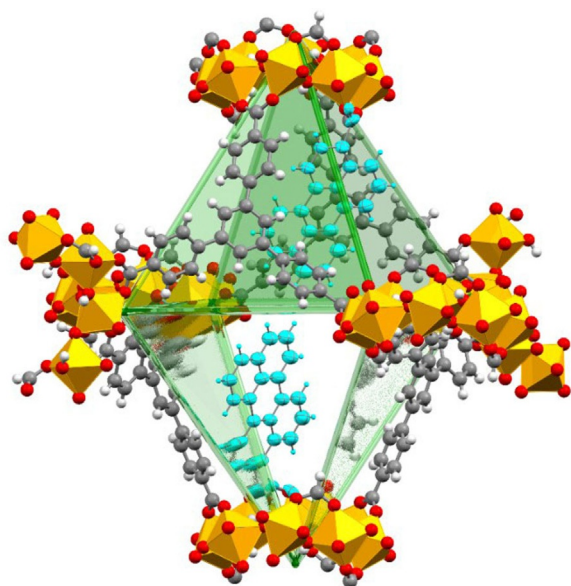


Figure 3. Representation of the single-crystal X-ray diffraction structure of MOF-520-PC1. The MOF cavity and framework ligands are emphasized with the green translucent planes. PC1 moieties are represented in blue ORTEP and Al-based SBUs in orange polyhedral.

Table 1. Summary of control experiments for reductive coupling reactions.^[a]

PC	PC [mol%]	Yield ^[b] [%]
PC1	0.5	68
PC2	0.5	63
PC1	2	75
PC2	3	81
MOF-520-PC1	0.9 (1.6) ^[c]	74
MOF-520-PC2	0.9 (2.8) ^[c]	82

[a] Conditions: **1a** (0.1 mmol), DIPEA (1.4 mmol), and different photocatalysts in CH_3CN/CH_3OH (3:2 v/v, 2 mL) at 30 °C, under N_2 were irradiated for 16 h (light-emitting diode (LED), $\lambda = 447$ nm). [b] Yields are calculated by means of 1H NMR spectroscopy with 1,3,5-trimethoxybenzene as an internal standard (I.S.) [c] PC incorporation within the structure is 44 and 77% for PC1 and PC2, respectively. Therefore, it should be considered that the PC concentration is estimated to be about 1.6 and 2.8 mol% for PC1 and PC2, respectively.

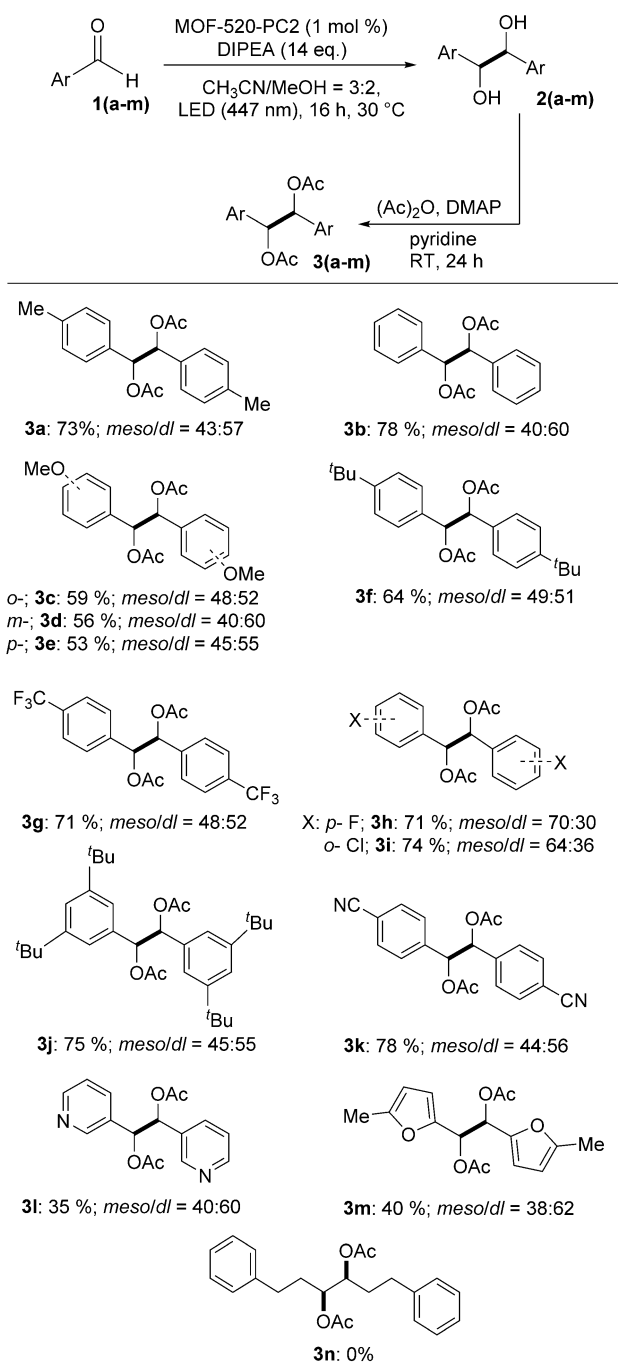
hyde **1 n**. Having outlined the scope for aldehydes, we next applied the MOF-520-PC2 catalyst to benzophenones and imines without further optimization (Scheme 3). In the case of imine reduction, up to 79% yield was found. The limit of the catalytic system starts to appear in the coupling of more bulky substrates and more challenging to reduce substrates, such as ketones and aliphatic aldehydes.^[26]

On the other hand, although there have been significant advances in the pinacol coupling reaction,^[27] the intermolecular cross-pinacol coupling that produces a single cross-coupled 1,2-diol selectively still remains a challenge.^[28] Strategies to address chemoselective control include prefunctionalization with stoichiometric quantities of metal salts, employing one coupling partner in large quantities, the use of highly functionalized carbonyl compounds,^[29] or exploiting differences in reactivity between coupling partners through an ionic mechanism.^[30] In this regard, to prove the effect of encapsulation of the photocatalysts in the MOF-520-PC2 on selectivity, we performed the heterocoupling of two different aldehydes, **1 b** and **1 j**, with marked differences in steric effects and compared them with homogeneous PC2.

The reactions were carried out by using an equimolar mixture of the two aldehydes. Moreover, irradiation for 8 h was used to better observe differences in reactivity. The crude reaction mixture, without further manipulation, was analyzed by means of ¹H NMR spectroscopy with an internal standard for quantification. In this way, the selectivity was not altered during the isolation procedure (Table S7 in the Supporting Information). Although in both cases a mixture of homo- (**2 j**, **2 b**) and heterocoupling (**2 o**) products were obtained, there was a remarkable difference in selectivity for the bulkier substrate, **2 j**. A product selectivity **2 b/2 j** value of 4.6 was obtained for MOF-520-PC2, whereas it was 1.0 for PC2. This 4.6-fold increase for **2 b** formation versus **2 j** suggests a size-exclusion effect of the cavities of MOF-520-PC2.

Recycling in batch

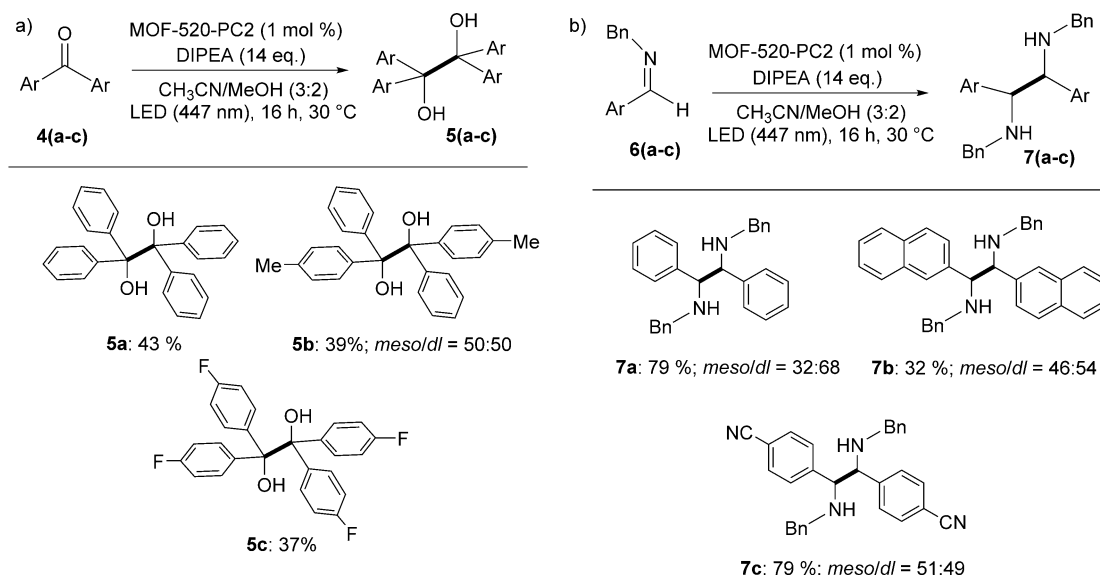
MOF-520-PC2 can be easily separated and recovered from the reaction mixture through filtration. Therefore, we studied the potential recycling of the catalysts after catalyzing the pinacol coupling of **1 a**. After washing twice with methanol and acetone, recycled MOF-520-PC2 was subjected to another catalytic run with the same substrate. The catalytic activity was maintained for the first two cycles (79 and 75%) and dropped in the third one to 34% yield of **2 a** (Table S5 in the Supporting Information). This reduction in yield was accompanied by a significant reduction in the crystallinity of the catalyst, as confirmed by PXRD analysis (Figure S11 in the Supporting Information). We rationalize that prolonged stirring used under the catalytic conditions may be responsible for the structural degradation of MOF-520-PC2, which then diminishes the catalytic activity, since the catalytic sites are no longer accessible to the organic substrates.



Scheme 2. Results obtained for the reductive coupling reactions of aromatic aldehydes catalyzed by MOF-520-PC2. Reaction conditions: MOF-520-PC2 (1 mol%), aldehyde (0.1 mmol), DIPEA (1.4 mmol), in CH₃CN/CH₃OH (*v/v* = 3:2, 2 mL) at 30 °C, under N₂ during 16 h of irradiation (LED, λ = 447 nm). Yields refer to products isolated; each substrate was run in three vials in parallel reactions that were combined after the reaction for isolation. DMAP = 4-dimethylaminopyridine.

Photocatalysis in flow

Taking advantage of the heterogeneous nature of MOF catalysts, we studied the potential use of MOF-520-PC2 as a photocatalyst under flow conditions.^[31,32] Indeed, flow chemistry has many advantages, such as easy scaling and automation.^[33]



Scheme 3. Results obtained for the reductive coupling reactions of a) benzophenones and b) aromatic imines, catalyzed by MOF-520-PC2. Reaction conditions: MOF-520-PC2 (1 mol%), ketone or imine (0.1 mmol), DIPEA (1.4 mmol), and CH₃CN/CH₃OH (3:2 v/v, 2 mL) at 30 °C, under N₂ during 16 h of irradiation (LED, $\lambda = 447$ nm). Yields refer to products isolated. Each substrate was run in two vials in parallel reactions that were combined after the reaction for isolation. Bn = benzyl.

However, scarce light penetration is probably the reason for the few applications of photocatalytic transformation by using heterogeneous materials under flow conditions.

The nature of the developed material (MOF-520-PC2) encouraged us to develop a heterogeneous photocatalytic system operative under flow conditions. We selected prototype substrates with different electronic properties, **1i** and **1a**, for testing. To set up the flow reactor, we prepared a 1% dilution of MOF-520-PC2 in Celite® and directly packed it into a column (20×0.6 cm) with glass beads to increase light harvesting of the photocatalyst (Figure 4, see the Supporting Information for further details). Packing was carried out under aerobic conditions without any particular precautions. The reaction mixture contained the substrate and electron donor under identical conditions to those already discussed and optimized for batch reactions. The photoreactor was irradiated perpendicular to the surface from two light sources (Kessil lamp, $\lambda = 450$ nm) at 180° to each other. The first solution containing **1i** (0.55 g) was pumped through the photoreactor (flow rate of 1.5 mL h⁻¹; Figure S12 in the Supporting Information), followed by **1a** (0.55 g) after washing. Notably, sample preparation and the photoreactions were performed in air, which further demonstrated the robustness of the catalytic system. As a result, the two consecutive 0.55 g scale reactions led to the isolation of products **3i** and **3a** in good overall yields (0.49 and 0.38 g, respectively, corresponding to 70 and 51% yield after two reactions, respectively; Figure 4), which validated the effectiveness of the system.

Photophysical and electrochemical characterization

To better understand the nature of the catalytic sites, we have investigated the photophysical and electrochemical properties of the as-synthesized MOFs and PCs.

First, optical spectroscopic studies give insights into potential interactions between perylenes, or perylenes and the MOF matrix. Diffuse reflectance spectra of PC1 and PC2 (Figure S13a and b in the Supporting Information) showed broad absorption bands characteristic of the perylene monomer and a sharper band at $\lambda \approx 430$ nm.^[34] In both cases, encapsulation in MOF-520 only induced minor changes in absorbance, which suggested that the electronic structure of the PC were not significantly altered in the solid state. Absorption and luminescence studies in solution, or suspensions in the case of MOFs, were more informative regarding potential aggregation processes (Figure 5 and Figure S14 in the Supporting Information). The UV/Vis absorption spectra of PC1 and PC2 show broad bands ($\lambda = 360$ –470 nm). In the case of PC1, the characteristic vibrational fine structure of the perylene is not resolved, even at concentrations as low as 1 μ M, whereas, in the case of PC2, characteristic vibronic spectra of perylene monomers are present (1–25 μ M). Presumably, the difference arises from different capacities of PC1 and PC2 to form π -stacking structures, which is likely to be more favorable for PC1, since the formation of carboxylic acid homodimers duplicates the size of the π -conjugated structure (Figure 5). This is in agreement with the fact that the presence of a base, such as DIPEA (5 mM), resolves the characteristic vibronic spectra of perylene monomers for PC1, since it disrupts the formation of homodimers. The UV/Vis features of PC1 and PC2 are located in the visible region, without overlap to the MOF-520 absorption of the BTB linkers ($\lambda =$

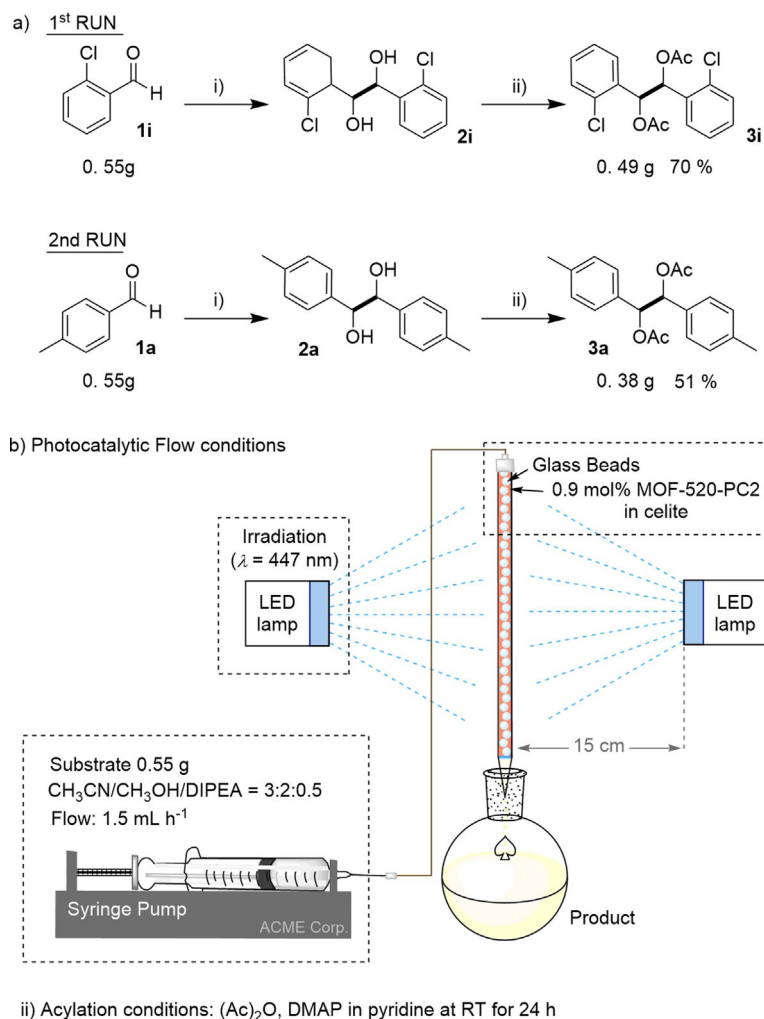


Figure 4. a) Consecutive photocatalytic reduction of aldehydes **1i** and **1a** to the corresponding pinacols under flow conditions with the same MOF-520-PC2/Celite® packed column. b) Schematic illustration of the experimental setup.

276 nm), facilitating analysis of the postmodified MOFs (Figure S14 in the Supporting Information).

Interestingly, in the absorption spectra of the MOF-520-PCs, perylene vibronic features are present for both cases; this suggests negligible perylene–perylen interactions or MOF–perylen interactions. To further understand the aggregation behavior of perylenes inside the MOF matrix, we also recorded fluorescence spectra of PCs in the concentration range from 1 to 100 μM , as well as suspensions of MOF-520-PCs. Similar to the UV/Vis absorption spectra, fluorescence spectra of PC1 showed unresolved vibronic features, which appeared in the presence of DIPEA and perfectly matched the spectrum of the suspended MOF-520-PC1. Also, the fluorescence spectra of PC2 and MOF-520-PC2 were informative. As the concentration increases, the luminescence vibronic bands at $\lambda = 445$ nm decrease and the feature at $\lambda = 475$ nm rises, revealing an aggregation process between perylene units, which are not revealed in the studied UV/Vis spectral range (Figure 5). Similar to the UV/Vis spectrum, the fluorescence spectrum of MOF-520-PC2 matches with that of PC2 only at low concentration (1 μM pho-

tocatalyst), which indicates that PC2 behaves as a monomer inside of the MOF-520.^[35]

Cyclic voltammetry (CV) experiments showed apparent differences between perylene precursors. The first reduction wave of PC2 is shifted by 340 mV to more negative potentials than that of PC1 ($E_{\text{PC2}}^0 = -1.80$ V and $E_{\text{PC1}}^0 = -1.45$ V, respectively). All redox values are given versus a standard calomel electrode (SCE), unless stated otherwise (Table 2 and Figure S13c in the Supporting Information). Although the cyclic voltammograms of the MOFs follow a similar trend to that of the perylene precursors, the interpretation is not straightforward. The CV results for MOF-520 show two reduction waves that shift to positive and negative redox potentials in MOF-520-PC1 and MOF-520-PC2, respectively (Figure S13d in the Supporting Information). We observed that the extension of the shifts depended on the perylene. The shift was more significant in the case of MOF-520-PC1, in which the perylene is electronically connected to the carboxylate and then to the aluminum centers. Conversely, for MOF-520-PC2, the perylene–Al centers are electronically disconnected by an alkyl spacer, which barely affects the redox process of the MOF.^[34] Neverthe-

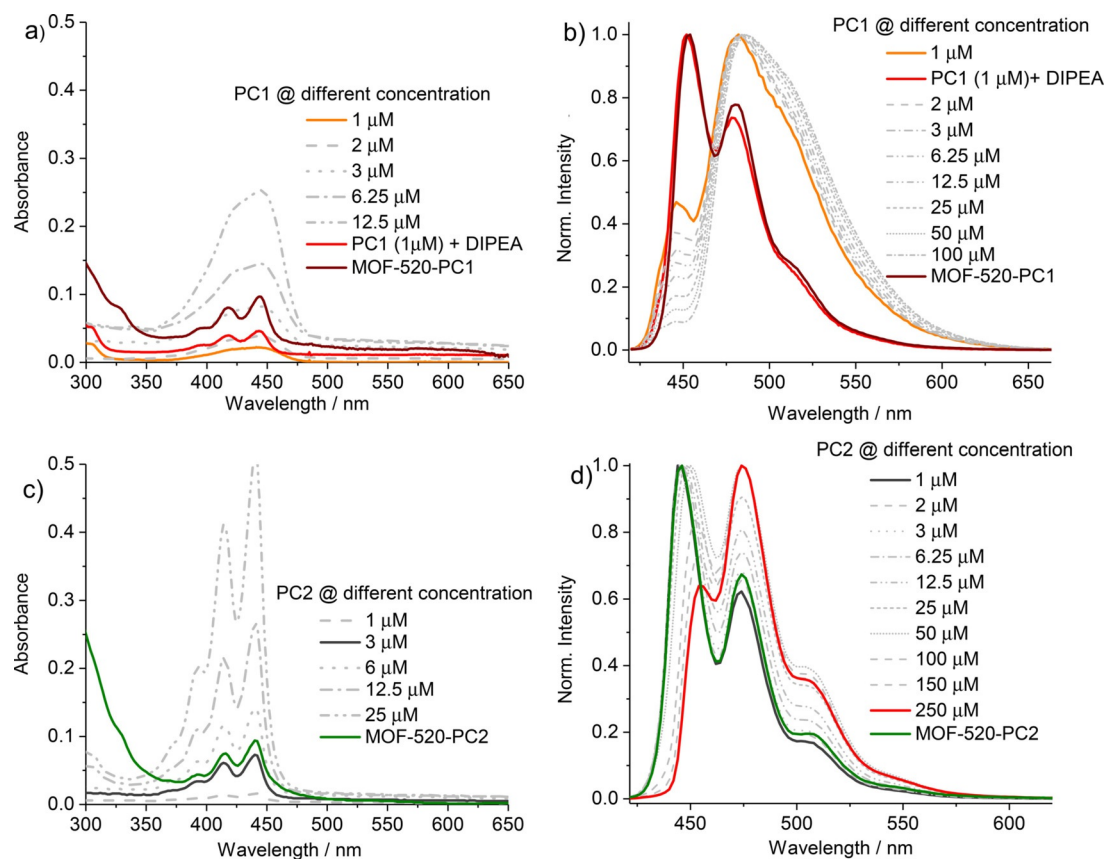


Figure 5. Absorption (a) and fluorescence (b) spectra of PC1 measured upon increasing its concentration and further compared with a suspension of MOF-520-PC1 (1 mg mL^{-1}). Absorption (c) and fluorescence (d) spectra of PC2 measured upon increasing its concentration and further compared with the same in the presence of DIPEA and MOF-520-PC2 (1 mg mL^{-1}) in suspension. Solvent, CH_3CN ; DIPEA (5 mM); $\lambda_{\text{ex}} = 410 \text{ nm}$.

less, because the absorption and fluorescence spectra do not undergo significant changes, we estimate that the redox potentials of PCs within the MOF do not significantly deviate from those of the free PCs. Therefore, we hypothesize that the redox difference between the two materials can be the ascribed as the main factor for the differences in catalysis.

Finally, we characterized the excited states by means of time-correlated single-photon counting in the solid state (Figure 6 and Table S8 in the Supporting Information). In both cases, the multiexponential lifetime decay of PCs is similar to that of the MOF-520-PCs (Table 2); the slowest $\tau_{1/2}$ is about

6 ns for PC1 and 8 ns for PC2.^[35a,36,37] This result, together with those previously reported, is in agreement with the fact that both PCs behave as isolated units inside the MOF-520.

Mechanistic studies

To gain insights into the reductive coupling reaction of aldehydes, we examined key steps of the catalytic cycle with the help of steady-state, time-resolved fluorescence quenching studies and transient spectroscopy experiments. To this end, we have focused our efforts on the model reaction of **1a** with MOF-520-PC2, in the absence and presence of DIPEA. As presented above, perylene PC2 inside MOF-520 behaves as a monomer, as determined by the absorption and emission spectra (Figures S15 and S17 in the Supporting Information).

The lifetime of the MOF-520-PC2* excited state was long enough to be quenched by DIPEA, as observed by the fluorescence (Figure S15 c and d in the Supporting Information) and excited-state lifetime quenching studies (Figure 7 c and d). Similar bimolecular quenching rate constants (k_q) were obtained by time-correlated single-photon counting for MOF-520-PC1 ($(6.0 \pm 0.3) \times 10^9 \text{ M}^{-1} \text{ s}^{-1}$, see Table S9 and the Supporting Information for calculation details) and MOF-520-PC2 ($(5.9 \pm 0.3) \times 10^9 \text{ M}^{-1} \text{ s}^{-1}$; Table S10 in the Supporting Information). Upon studying **1a** as a quencher, we could not observe quenching

Table 2. Summary of the redox processes and excited-state lifetimes in solution.

Sample	$\lambda_{\text{abs}}^{[a]}$ [nm]	$\lambda_{\text{em}}^{[b]}$ [nm]	$\tau_1^{[c]}$ [ns]	$E_{1/2}^{(0/-)}$ (V vs. SCE)	$E^{(+/)}$
PC1	442	452	4.5	-1.45	1.25
PC2	440	446	4.2	-1.80	1.0
MOF-520	275	390	3.5	-	-
MOF-520-PC1	445	454	6	-	-
MOF-520-PC2	440	448	5.2	-	-

[a] Values obtained from the maximum absorption band. [b] Values obtained from the maximum fluorescence band. [c] Lifetimes were obtained from the single-exponential fit at λ_{em} . Absorption and fluorescence spectra were recorded in $\text{CH}_3\text{CN}/\text{CH}_3\text{OH}$ (3:2 v/v).

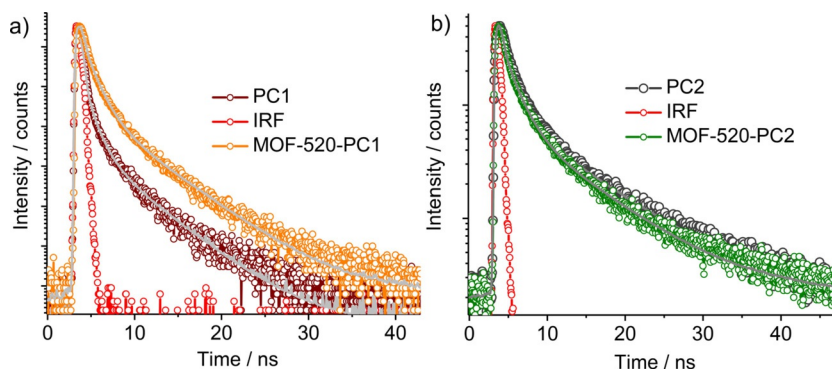


Figure 6. Normalized solid-state lifetime decay of a) PC1 and MOF-520-PC1, and b) PC2 and MOF-520-PC2, as measured by time-correlated single-photon counting and its exponential fits. $\lambda_{\text{ex}} = 470$ nm laser, $\lambda_{\text{em}} = 560$ nm. (IRF = instrument response function from the laser source.)

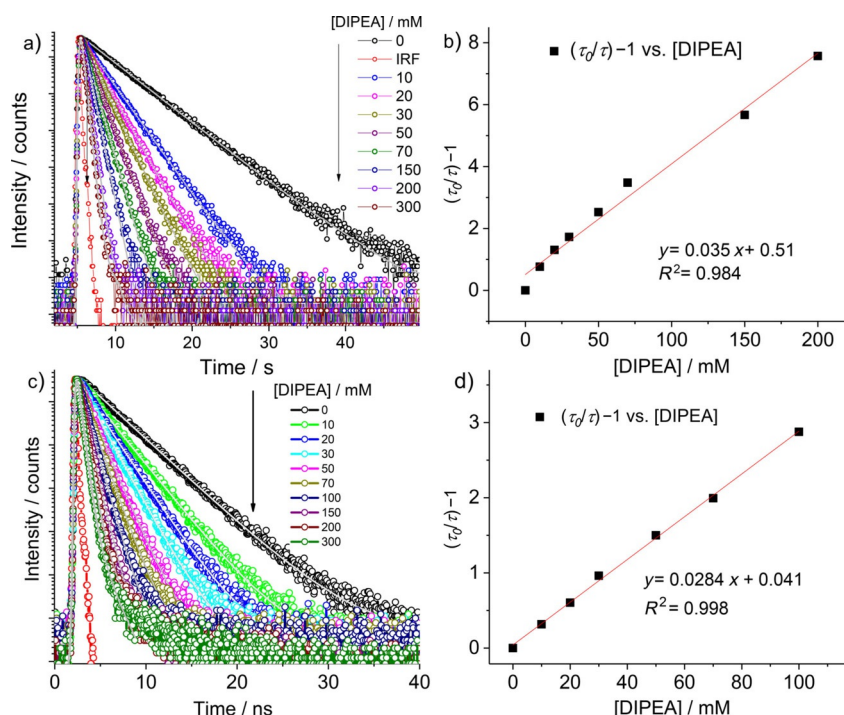
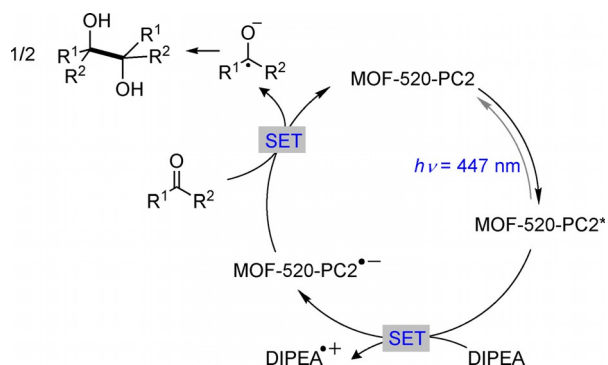


Figure 7. Titration lifetime decay of MOF-520-PC1 (a) and MOF-520-PC2 (c) with DIPEA in a mixture of $\text{CH}_3\text{CN}/\text{CH}_3\text{OH}$ (3:2 v/v, 2 mL). $\lambda_{\text{ex}} = 405$ nm laser, $\lambda_{\text{em}} = 460$ nm. Stern-Volmer quenching analysis of the changes in lifetimes as a function of [DIPEA] for MOF-520-PC1 (b) and MOF-520-PC2 (d). The sample was prepared as a fine suspension after ball milling, cell path length 1 cm, $T = 25^\circ\text{C}$.

at concentrations relevant for catalysis (Figure S16 in the Supporting Information). Redox values of DIPEA and PC2* suggest that a single electron transfer (SET) between them is thermodynamically feasible ($E_{(\text{DIPEA})^0} = 0.72$ V^[38] and $E_{(\text{PC2}^*/\text{PC2}^-)} = 1.0$ V vs. SCE; Figure S17b,d in the Supporting Information). Likewise, SET from DIPEA to MOF-520-PC2* should also be thermodynamically feasible.^[39] Nevertheless, the formation of the radical anion of the photosensitizer can be observed by means of millisecond transient absorption spectroscopy. Indeed, in the case of PC2, the PC2* excited state follows the formation of the PC2⁻ radical anion in the presence of DIPEA (Figure S18a in the Supporting Information) with a clear absorption band at $\lambda = 570$ nm. Monitoring the radical anion at $\lambda = 570$ nm presented a biexponential decay time of about 0.75 and 3.6 ms (Table S11 in the Supporting Information), which could be ra-

tionalized as recombination on the millisecond timescale. Under the same conditions, but in the presence of **1a**, the decays are reduced to 0.44 and 3.0 ms (Table S11 in the Supporting Information).

Likewise, in the case of MOF-520-PC2, the evolution of the radical anion can be followed at $\lambda = 570$ nm in the presence of DIPEA, but with a faster decay time than that in the case of PC2 in solution ($\langle \tau \rangle = 0.25$ ms). By adding **1a** to the same cuvette, the intensity of the signal at $\lambda = 570$ nm is reduced by more than half, which suggests SET between the radical anion by **1a** (Figure S18d in the Supporting Information). Therefore, the proposed mechanism of the photocatalytic reductive coupling reaction starts with the excitation of the PC ($\lambda = 447$ nm), which undergoes reductive quenching with DIPEA to afford MOF-520-PC⁻. Successive SET to the substrate results in the



Scheme 4. Proposed mechanism for the visible-light-driven reductive coupling reaction of aromatic aldehydes, acetophenones, and imines with MOF-520-PC2.

reduction of the carbonyl group, followed by the C–C homocoupling reaction (Scheme 4).^[26]

Conclusions

We reported a straightforward postsynthetic transformation of MOF-520 with two differently substituted perylene molecules to introduce a photoredox functionality to the material. As determined by the redox potential, differences in the catalytic activity between the two materials can be ascribed to the redox potential differences between the reduced state of the PCs; PC2 is more reducing than that of PC1. The new heterogeneous organo-photocatalysts revealed efficient light-driven reductive coupling of aldehydes, ketones, and imines to give 1,2-diols and 1,2-diamines, with similar catalytic activity to the homogeneous counterpart, but with recyclable capacity. Moreover, continuous-flow photocatalytic conditions highlight the potential of this technique through the proof of gram-scale catalytic transformation and reusability. Combining steady-state and time-resolved spectroscopy revealed that perylenes immobilized in MOF-520 acted as an isolated unit, and therefore, the catalytic activity could be exclusively ascribed to the perylene monomer, whereas in the homogeneous phase the potential aggregation of perylenes complicated the assignment of the real catalytically active species. We envision that this study will open up new perspectives in the design of heterogeneous PCs through further developments of photocatalytically active materials based on the straightforward crystal-to-crystal transformation of MOF-520 and potential light-driven organic transformations under flow conditions.

Experimental Section

Figures, tables, text, and CIF files reporting crystal data, experimental details, and the results of catalysis can be found in the Supporting Information.

CCDC 1972303 (MOF-520-PC1) contain the supplementary crystallographic data for this paper. These data are provided free of charge by The Cambridge Crystallographic Data Centre.

Acknowledgements

We thank the ICIQ Foundation, the European Research Foundation for project ERC-2014-CoG 648304 (J.L.-F.), MINECO (CTQ2016-80038-R; J.L.-F.), and AGAUR 2017-SGR-1647 (J.L.-F.) for funding. S.S.M. and N.K. are grateful to Marie-Curie COFUND and JyC for postdoctoral scholarships, respectively.

Conflict of interest

The authors declare no conflict of interest.

Keywords: C–C coupling · crystal-to-crystal synthesis · metal-organic frameworks · photochemistry · X-ray diffraction

- [1] a) K. L. Skubi, T. R. Blum, T. P. Yoon, *Chem. Rev.* **2016**, *116*, 10035–10074; b) B. König, *Eur. J. Org. Chem.* **2017**, 1979–1981; c) T. P. Yoon, M. A. Ischay, J. Du, *Nat. Chem.* **2010**, *2*, 527; d) L. Marzo, S. K. Pagire, O. Reiser, B. König, *Angew. Chem. Int. Ed.* **2018**, *57*, 10034–10072; *Angew. Chem.* **2018**, *130*, 10188–10228; e) *Visible Light Photocatalysis in Organic Chemistry* (Eds.: C. R. Stephenson, T. P. Yoon, D. W. MacMillan), Wiley-VCH, Weinheim, **2018**; f) L. Buzzetti, G. E. M. Crisenza, P. Melchiorre, *Angew. Chem. Int. Ed.* **2019**, *58*, 3730–3747; *Angew. Chem.* **2019**, *131*, 3768–3786.
- [2] a) C. K. Prier, D. A. Rankic, D. W. C. MacMillan, *Chem. Rev.* **2013**, *113*, 5322–5363; b) A. Hossain, A. Bhattacharyya, O. Reiser, *Science* **2019**, *364*, eaav9713; c) D. M. Arias-Rotondo, J. K. McCusker, *Chem. Soc. Rev.* **2016**, *45*, 5803–5820; d) T. Koike, M. Akita, *Inorg. Chem. Front.* **2014**, *1*, 562–576; e) O. S. Wenger, *Coord. Chem. Rev.* **2015**, *282–283*, 150–158; f) Q. M. Kainz, C. D. Matier, A. Bartoszewicz, S. L. Zultanski, J. C. Peters, G. C. Fu, *Science* **2016**, *351*, 681; g) A. Sagadevan, V. P. Charpe, A. Ragupathi, K. C. Hwang, *J. Am. Chem. Soc.* **2017**, *139*, 2896–2899; h) S. Paria, O. Reiser, *ChemCatChem* **2014**, *6*, 2477–2483; i) Y. Zhang, M. Schulz, M. Wächter, M. Karnahl, B. Dietzek, *Coord. Chem. Rev.* **2018**, *356*, 127–146.
- [3] a) N. A. Romero, D. A. Nicewicz, *Chem. Rev.* **2016**, *116*, 10075–10166; b) C. Stephenson, T. Yoon, *Acc. Chem. Res.* **2016**, *49*, 2059–2060; c) M. Silvi, E. Arceo, I. D. Jurberg, C. Cassani, P. Melchiorre, *J. Am. Chem. Soc.* **2015**, *137*, 6120–6123; d) B. Schweitzer-Chaput, M. A. Horwitz, E. de Pedro Beato, P. Melchiorre, *Nat. Chem.* **2019**, *11*, 129–135; e) J. C. Theriot, C. H. Lim, H. Yang, M. D. Ryan, C. B. Musgrave, G. M. Miyake, *Science* **2016**, *352*, 1082–1086; f) B. G. McCarthy, R. M. Pearson, C.-H. Lim, S. M. Sartor, N. H. Damrauer, G. M. Miyake, *J. Am. Chem. Soc.* **2018**, *140*, 5088–5101; g) T.-Y. Shang, L.-H. Lu, Z. Cao, Y. Liu, W.-M. He, B. Yu, *Chem. Commun.* **2019**, *55*, 5408–5419; h) O. S. Wenger, *J. Am. Chem. Soc.* **2018**, *140*, 13522–13533; i) C. B. Larsen, O. S. Wenger, *Chem. Eur. J.* **2018**, *24*, 2039–2058.
- [4] a) S. Okamoto, K. Kojiyama, H. Tsujioka, A. Sudo, *Chem. Commun.* **2016**, *52*, 11339–11342; b) S. Okamoto, R. Ariki, H. Tsujioka, A. Sudo, *J. Org. Chem.* **2017**, *82*, 9731–9736.
- [5] a) M. Silva, M. J. F. Calvete, N. P. F. Gonçalves, H. D. Burrows, M. Sarakha, A. Fernandes, M. F. Ribeiro, M. E. Azenha, M. M. Pereira, *J. Hazard. Mater.* **2012**, *233–234*, 79–88; b) M. Silva, M. E. Azenha, M. M. Pereira, H. D. Burrows, M. Sarakha, C. Forano, M. F. Ribeiro, A. Fernandes, *Appl. Catal. B* **2010**, *100*, 1–9.
- [6] a) A. Corma, H. Garcia, *Chem. Commun.* **2004**, 1443–1459; b) Z. J. Wang, S. Ghasimi, K. Landfester, K. A. I. Zhang, *Chem. Mater.* **2015**, *27*, 1921–1924; c) W.-J. Yoo, S. Kobayashi, *Green Chem.* **2014**, *16*, 2438–2442.
- [7] Y. Liu, G. Zhu, B. Ge, H. Zhou, A. Yuan, X. Shen, *CrystEngComm* **2012**, *14*, 6264–6270.
- [8] a) H.-C. J. Zhou, S. Kitagawa, *Chem. Soc. Rev.* **2014**, *43*, 5415–5418; b) J. Liu, L. Chen, H. Cui, J. Zhang, L. Zhang, C.-Y. Su, *Chem. Soc. Rev.* **2014**, *43*, 6011–6061; c) K. Sumida, D. L. Rogow, J. A. Mason, T. M. McDonald, E. D. Bloch, Z. R. Herm, T.-H. Bae, J. R. Long, *Chem. Rev.* **2012**, *112*, 724–781.
- [9] a) K. G. M. Laurier, F. Vermoortele, R. Ameloot, D. E. De Vos, J. Hofkens, M. B. J. Roefsaers, *J. Am. Chem. Soc.* **2013**, *135*, 14488–14491; b) D.

- Wang, R. Huang, W. Liu, D. Sun, Z. Li, *ACS Catal.* **2014**, *4*, 4254–4260; c) Y. Zhang, J. Guo, L. Shi, Y. Zhu, K. Hou, Y. Zheng, Z. Tang, *Sci. Adv.* **2017**, *3*, e1701162.
- [10] a) C. Wang, Z. Xie, K. E. deKrafft, W. Lin, *J. Am. Chem. Soc.* **2011**, *133*, 13445–13454; b) X. Yu, S. M. Cohen, *Chem. Commun.* **2015**, *51*, 9880–9883; c) Y. Fang, X. Li, F. Li, X. Lin, M. Tian, X. Long, X. An, Y. Fu, J. Jin, J. Ma, *J. Power Sources* **2016**, *326*, 50–59; d) J. A. Johnson, X. Zhang, T. C. Reeson, Y.-S. Chen, J. Zhang, *J. Am. Chem. Soc.* **2014**, *136*, 15881–15884.
- [11] P. Wu, C. He, J. Wang, X. Peng, X. Li, Y. An, C. Duan, *J. Am. Chem. Soc.* **2012**, *134*, 14991–14999.
- [12] L. Zeng, T. Liu, C. He, D. Shi, F. Zhang, C. Duan, *J. Am. Chem. Soc.* **2016**, *138*, 3958–3961.
- [13] a) D. Shi, C. He, B. Qi, C. Chen, J. Niu, C. Duan, *Chem. Sci.* **2015**, *6*, 1035–1042; b) X. Wang, W. Lu, Z.-Y. Gu, Z. Wei, H.-C. Zhou, *Chem. Commun.* **2016**, *52*, 1926–1929.
- [14] a) J.-R. Li, R. J. Kuppler, H.-C. Zhou, *Chem. Soc. Rev.* **2009**, *38*, 1477–1504; b) K. Tan, S. Zuluaga, E. Fuentes, E. C. Mattson, J.-F. Veyan, H. Wang, J. Li, T. Thonhauser, Y. J. Chabal, *Nat. Commun.* **2016**, *7*, 13871.
- [15] a) L. E. Kreno, K. Leong, O. K. Farha, M. Allendorf, R. P. Van Duyne, J. T. Hupp, *Chem. Rev.* **2012**, *112*, 1105–1125; b) J. J. Gassensmith, J. Y. Kim, J. M. Holcroft, O. K. Farha, J. F. Stoddart, J. T. Hupp, N. C. Jeong, *J. Am. Chem. Soc.* **2014**, *136*, 8277–8282; c) P. Wu, Y. Liu, Y. Liu, J. Wang, Y. Li, W. Liu, J. Wang, *Inorg. Chem.* **2015**, *54*, 11046–11048; d) F.-Y. Yi, D. Chen, M.-K. Wu, L. Han, H.-L. Jiang, *ChemPlusChem* **2016**, *81*, 675–690.
- [16] a) Y. Cui, Y. Yue, G. Qian, B. Chen, *Chem. Rev.* **2012**, *112*, 1126–1162; b) J. Yu, Y. Cui, C.-D. Wu, Y. Yang, B. Chen, G. Qian, *J. Am. Chem. Soc.* **2015**, *137*, 4026–4029; c) B. Chen, L. Wang, Y. Xiao, F. R. Fronczek, M. Xue, Y. Cui, G. Qian, *Angew. Chem. Int. Ed.* **2009**, *48*, 500–503; *Angew. Chem.* **2009**, *121*, 508–511.
- [17] a) H. Zheng, Y. Zhang, L. Liu, W. Wan, P. Guo, A. M. Nyström, X. Zou, *J. Am. Chem. Soc.* **2016**, *138*, 962–968; b) C. Doonan, R. Riccò, K. Liang, D. Bradshaw, P. Falcaro, *Acc. Chem. Res.* **2017**, *50*, 1423–1432.
- [18] a) Y.-B. Huang, J. Liang, X.-S. Wang, R. Cao, *Chem. Soc. Rev.* **2017**, *46*, 126–157; b) V. Pascanu, G. González Miera, A. K. Inge, B. Martín-Matute, *J. Am. Chem. Soc.* **2019**, *141*, 7223–7234; c) A. Dhakshinamoorthy, Z. Li, H. Garcia, *Chem. Soc. Rev.* **2018**, *47*, 8134–8172; d) N. Huang, K. Wang, H. Drake, P. Cai, J. Pang, J. Li, S. Che, L. Huang, Q. Wang, H.-C. Zhou, *J. Am. Chem. Soc.* **2018**, *140*, 6383–6390; e) N. Huang, S. Yuan, H. Drake, X. Yang, J. Pang, J. Qin, J. Li, Y. Zhang, Q. Wang, D. Jiang, H.-C. Zhou, *J. Am. Chem. Soc.* **2017**, *139*, 18590–18597; f) Z. Li, A. W. Peters, A. E. Platero-Prats, J. Liu, C.-W. Kung, H. Noh, M. R. DeStefano, N. M. Schweitzer, K. W. Chapman, J. T. Hupp, O. K. Farha, *J. Am. Chem. Soc.* **2017**, *139*, 15251–15258; g) J. Liu, J. Ye, Z. Li, K.-i. Otake, Y. Liao, A. W. Peters, H. Noh, D. G. Truhlar, L. Gagliardi, C. J. Cramer, O. K. Farha, J. T. Hupp, *J. Am. Chem. Soc.* **2018**, *140*, 11174–11178; h) T. Zhang, K. Manna, W. Lin, *J. Am. Chem. Soc.* **2016**, *138*, 3241–3249; i) T. Drake, P. Ji, W. Lin, *Acc. Chem. Res.* **2018**, *51*, 2129–2138.
- [19] a) X. Yu, L. Wang, S. M. Cohen, *CrystEngComm* **2017**, *19*, 4126–4136; b) L. Zeng, X. Guo, C. He, C. Duan, *ACS Catal.* **2016**, *6*, 7935–7947; c) W. Tu, Y. Xu, S. Yin, R. Xu, *Adv. Mater.* **2018**, *30*, 1707582; d) C. Xu, R. Fang, R. Luque, L. Chen, Y. Li, *Coord. Chem. Rev.* **2019**, *388*, 268–292; e) Y.-Y. Zhu, G. Lan, Y. Fan, S. S. Veroneau, Y. Song, D. Micheroni, W. Lin, *Angew. Chem. Int. Ed.* **2018**, *57*, 14090–14094; *Angew. Chem.* **2018**, *130*, 14286–14290; f) R. Xu, Z. Cai, G. Lan, W. Lin, *Inorg. Chem.* **2018**, *57*, 10489–10493; g) T. Zhang, W. Lin, *Chem. Soc. Rev.* **2014**, *43*, 5982–5993; h) J.-L. Wang, C. Wang, W. Lin, *ACS Catal.* **2012**, *2*, 2630–2640.
- [20] a) S. Lee, E. A. Kapustin, O. M. Yaghi, *Science* **2016**, *353*, 808–811; b) F. Gándara, H. Furukawa, S. Lee, O. M. Yaghi, *J. Am. Chem. Soc.* **2014**, *136*, 5271–5274; c) E. A. Kapustin, S. Lee, A. S. Alshammari, O. M. Yaghi, *ACS Cent. Sci.* **2017**, *3*, 662–667; d) X. Pei, H.-B. Bürgi, E. A. Kapustin, Y. Liu, O. M. Yaghi, *J. Am. Chem. Soc.* **2019**, *141*, 18862–18869.
- [21] a) R. E. Cook, B. T. Phelan, R. J. Kamire, M. B. Majewski, R. M. Young, M. R. Wasielewski, *J. Phys. Chem. A* **2017**, *121*, 1607–1615; b) F. M. Winnik, *Chem. Rev.* **1993**, *93*, 587–614; c) A. Aster, G. Licari, F. Zinna, E. Brun, T. Kumpulainen, E. Tajkhorshid, J. Lacour, E. Vauthey, *Chem. Sci.* **2019**, *10*, 10629–10639; d) Y. Huang, J. Xing, Q. Gong, L.-C. Chen, G. Liu, C. Yao, Z. Wang, H.-L. Zhang, Z. Chen, Q. Zhang, *Nat. Commun.* **2019**, *10*, 169; e) F. Ito, Y. Kogasaka, K. Yamamoto, *J. Phys. Chem. B* **2013**, *117*, 3675–3681; f) A. Furube, M. Murai, Y. Tamaki, S. Watanabe, R. Katoh, *J. Phys. Chem. A* **2006**, *110*, 6465–6471; g) Y. Nakamura, T. Nakazato, T. Kamatsuka, H. Shinokubo, Y. Miyake, *Chem. Eur. J.* **2019**, *25*, 10571–10574; h) M. Bonchio, Z. Syrgiannis, M. Burian, N. Marino, E. Pizzolato, K. Dirian, F. Rigodanza, G. A. Volpato, G. La Ganga, N. Demitri, S. Berardi, H. Amenitsch, D. M. Guldi, S. Caramori, C. A. Bignozzi, A. Sartorel, M. Prato, *Nat. Chem.* **2019**, *11*, 146–153; i) A. S. Weingarten, R. V. Kazantsev, L. C. Palmer, M. McClendon, A. R. Koltanow, A. P. S. Samuel, D. J. Kiebalá, M. R. Wasielewski, S. I. Stupp, *Nat. Chem.* **2014**, *6*, 964–970; j) X. Feng, P. Liao, J. Jiang, J. Shi, Z. Ke, J. Zhang, *ChemPhotoChem* **2019**, *3*, 1014–1019; k) E. Peris, *Chem. Commun.* **2016**, *52*, 5777–5787; l) S. Ibáñez, M. Poyatos, E. Peris, *Angew. Chem. Int. Ed.* **2018**, *57*, 16816–16820; *Angew. Chem.* **2018**, *130*, 17058–17062; m) S. Ibáñez, M. Poyatos, E. Peris, *Organometallics* **2017**, *36*, 1447–1451; n) S. Ibáñez, E. Peris, *Chem. Eur. J.* **2019**, *25*, 8254–8258.
- [22] a) K. C. Nicolaou, J. J. Liu, Z. Yang, H. Ueno, E. J. Sorensen, C. F. Clai-borne, R. K. Guy, C. K. Hwang, M. Nakada, P. G. Nantermet, *J. Am. Chem. Soc.* **1995**, *117*, 634–644; b) M. Nazaré, H. Waldmann, *Angew. Chem. Int. Ed.* **2000**, *39*, 1125–1128; *Angew. Chem.* **2000**, *112*, 1171–1174.
- [23] a) R. M. Archer, M. Hutchby, C. L. Winn, J. S. Fossey, S. D. Bull, *Tetrahe-dron* **2015**, *71*, 8838–8847; b) R. A. Kleinnijenhuis, B. J. J. Timmer, G. Lut-teke, J. M. M. Smits, R. de Gelder, J. H. van Maarseveen, H. Hiemstra, *Chem. Eur. J.* **2016**, *22*, 1266–1269; c) H. Huo, C. Fu, K. Harms, E. Meg-gers, *J. Am. Chem. Soc.* **2014**, *136*, 2990–2993.
- [24] a) A. Call, C. Casadevall, F. Acuña-Parés, A. Casitas, J. Lloret-Fillol, *Chem. Sci.* **2017**, *8*, 4739–4749; b) D. W. Wakerley, E. Reisner, *Energy Environ. Sci.* **2015**, *8*, 2283–2295.
- [25] N. Plumeré, O. Rüdiger, A. A. Oughli, R. Williams, J. Vivekananthan, S. Pöller, W. Schuhmann, W. Lubitz, *Nat. Chem.* **2014**, *6*, 822.
- [26] M. Nakajima, E. Fava, S. Loescher, Z. Jiang, M. Rueping, *Angew. Chem. Int. Ed.* **2015**, *54*, 8828–8832; *Angew. Chem.* **2015**, *127*, 8952–8956.
- [27] X.-F. Duan, J.-X. Feng, G.-F. Zi, Z.-B. Zhang, *Synthesis* **2009**, *2009*, 277–282.
- [28] a) T. Hirao in *Metal Catalyzed Reductive C–C Bond Formation: A Depart-ure from Preformed Organometallic Reagents* (Ed.: M. J. Krische), Springer, Berlin, **2007**, pp. 53–75; b) B. S. Terra, F. Macedo, Jr., *ChemInform* **2012**, *43*, https://doi.org/10.1002/chin.201216251.
- [29] a) R. L. Danheiser, A. L. Helgason, *J. Am. Chem. Soc.* **1994**, *116*, 9471–9479; b) J. H. Freudenberger, A. W. Konradi, S. F. Pedersen, *J. Am. Chem. Soc.* **1989**, *111*, 8014–8016.
- [30] M. Takeda, A. Mitsui, K. Nagao, H. Ohmiya, *J. Am. Chem. Soc.* **2019**, *141*, 3664–3669.
- [31] a) A. Sachse, R. Ameloot, B. Coq, F. Fajula, B. Coasne, D. De Vos, A. Galar-neau, *Chem. Commun.* **2012**, *48*, 4749–4751; b) V. Pascanu, P. R. Hansen, A. Bermejo Gómez, C. Ayats, A. E. Platero-Prats, M. J. Johansson, M. À. Pericàs, B. Martín-Matute, *ChemSusChem* **2015**, *8*, 123–130.
- [32] D. Cambié, C. Bottecchia, N. J. W. Straathof, V. Hessel, T. Noël, *Chem. Rev.* **2016**, *116*, 10276–10341.
- [33] C. Sambiasi, T. Noël, *Trends Chem.* **2020**, *2*, 92–106.
- [34] J. Merz, A. Steffen, J. Nitsch, J. Fink, C. B. Schürger, A. Friedrich, I. Krum-menacher, H. Braunschweig, M. Moos, D. Mims, C. Lambert, T. B. Marder, *Chem. Sci.* **2019**, *10*, 7516–7534.
- [35] a) A. K. Chaudhari, J.-C. Tan, *Nanoscale* **2018**, *10*, 3953–3960; b) M. D. Al-lendorf, C. A. Bauer, R. K. Bhakta, R. J. T. Houk, *Chem. Soc. Rev.* **2009**, *38*, 1330–1352; c) I. A. Fedorov, Y. N. Zhuravlev, V. P. Berveno, *J. Chem. Phys.* **2013**, *138*, 094509.
- [36] M. Müller, A. Devaux, C.-H. Yang, L. De Cola, R. A. Fischer, *Photochem. Photobiol. Sci.* **2010**, *9*, 846–853.
- [37] C. Dietl, H. Hintz, B. Rühle, J. Schmedt auf der Günne, H. Langhals, S. Wuttke, *Chem. Eur. J.* **2015**, *21*, 10714–10720.
- [38] G. J. Barbante, N. Kebede, C. M. Hindson, E. H. Doeven, E. M. Zammit, G. R. Hanson, C. F. Hogan, P. S. Francis, *Chem. Eur. J.* **2014**, *20*, 14026–14031.
- [39] a) A. K. Pal, C. Li, G. S. Hanan, E. Zysman-Colman, *Angew. Chem. Int. Ed.* **2018**, *57*, 8027–8031; *Angew. Chem.* **2018**, *130*, 8159–8163; b) J. S. Beckwith, B. Lang, J. Grilj, E. Vauthey, *J. Phys. Chem. Lett.* **2019**, *10*, 3688–3693.

Manuscript received: February 20, 2020

Revised manuscript received: April 3, 2020

Accepted manuscript online: April 29, 2020

Version of record online: June 8, 2020